Original Research

Mesenchymal stem cells–microvesicle-miR-451a ameliorate early diabetic kidney injury by negative regulation of P15 and P19

Ling Zhong[1,2], Guangneng Liao[1], Xiaojiao Wang[1], Lan Li[1], Jie Zhang[1], Younan Chen[1], Jingping Liu[1], Shuyun Liu[1], Lingling Wei[3], Wengeng Zhang[4] and Yanrong Lu[1]

[1]Key Lab of Transplant Engineering and Immunology, NHFPC, West China Hospital, Sichuan University, Chengdu, Sichuan 610041, China; [2]Department of Clinical and Experimental Medicine, Sichuan Academy of Medical Sciences and Sichuan Provincial People's Hospital, School of Medicine, University of Electronic Science and Technology of China, Chengdu, Sichuan 610072, China; [3]Institute of Organ Transplantation, Sichuan Academy of Medical Sciences and Sichuan Provincial People's Hospital, School of Medicine, University of Electronic Science and Technology of China, Chengdu, Sichuan 610072, China; [4]Precision Medicine Key Laboratory of Sichuan Province & Precision Medicine Center, West China Hospital, Sichuan University, Chengdu, Sichuan 610041, China
Corresponding authors: Yanrong Lu. Email: luyanrong@scu.edu.cn; Wengeng Zhang. Email: wengengzhang@cd120.com

Impact statement

The mechanism of MSCs repairing the injured kidney in diabetic nephropathy is not yet clear. In the research, MVs showed the same surface markers as MSCs but much higher MiR-451a expression. miR-451a was decreased in both injured HK-2 cells and kidneys. MV-miR-451a stimulated the cell proliferation and viability in vitro and promoted structural and functional improvements of injured kidney in vivo. Infusion of MV-miR-451a ameliorated EMT by reducing α-SMA and increasing E-cadherin. These effects relied on the improved cell cycle arrest and the down-regulation of P15 and P19 via miR-451a binding to their 3′-UTR region. This study demonstrated that MSC–MV-miR-451a could specifically inhibit cell cycle inhibitors to restart the blocked cell cycle and reverse EMT in vivo and in vitro. Therefore, miR-451a may be a new target for DN therapy.

Abstract

Microvesicles (MVs) from mesenchymal stem cells (MSCs) have been reported as a new communicated way between cells. This study evaluated the influence and underlying mechanism of MVs-shuttled miR-451a on renal fibrosis and epithelial mesenchymal transformation (EMT) in diabetic nephropathy (DN) with hyperuricemia. MVs were isolated from MSCs-cultured medium by gradient ultracentrifugation. The level of miR-451a in MSCs and MVs was analyzed by qPCR. The changes of miR-451a, E-cadherin, α-SMA, P15INK4b (P15), and P19INK4d (P19) were measured in hyperglycosis and hyperuricemia-induced cell (HK-2) and mouse models. The changes of cell cycle were analyzed by flow cytometry. The ability of proliferation and viability was measured by BrdU and CCK8, respectively. Dual-luciferase reporter assays were conducted to determine the target binding sites. The renal function and histological changes of mice were analyzed. MVs showed the same surface markers as MSCs but much higher miR-451a expression (4.87 ± 2.03 fold higher than MSCs). miR-451a was decreased to $26\% \pm 11\%$ and $6.7\% \pm 0.82\%$ in injured HK-2 cells and kidney, respectively. MV-miR-451a enhanced the HK2 cells proliferation and viability in vitro, and decreased the morphologic and functional injury of kidney in vivo. Moreover, infusion of MV-miR-451a reduced the level of α-SMA and raised E-cadherin expression. These effects were responsible for the improved arrested cell cycle and down-regulation of P15 and P19 via miR-451a targeting their 3′-UTR sites. This study demonstrated that MSC–MV-miR-451a could inhibit cell cycle inhibitors P15 and P19 to restart the blocked cell cycle and reverse EMT in vivo and in vitro, and thus miR-451a is potentially a new target for DN therapy.

Keywords: Mesenchymal stem cells, microvesicles, miR-451a, cell cycle, epithelial mesenchymal transformation

Experimental Biology and Medicine **2018; 243: 1233–1242. DOI: 10.1177/1535370218819726**

Introduction

Diabetes can cause a variety of chronic serious problems in multiple organs, including kidneys and eyes. While diabetic retinopathy is not life-threatening, diabetic nephropathy (DN) is the leading cause of death in patients suffering from diabetes.[1] The main pathological changes of DN are glomerular sclerosis and renal tubular interstitial fibrosis, in which the severity of interstitial fibrosis is more important

in determining patient prognosis. There are no targeted or specific drugs for the treatment of DN, especially renal fibrosis.[2] Thus, the discovery of effective targets to delay or even reverse the disease process is critical but remains challenging.

Renal fibrosis is manifested by the injury of renal tubular epithelial cells, chronic inflammation and accumulated extracellular matrix. Epithelial mesenchymal transformation (EMT) is vital in the pathological process of renal fibrosis. Renal fibrosis is usually accompanied with cell cycle arrest.[3] Both P15INK4b (P15) and P19INK4d (P19) belong to the INK4 protein family of the cyclin kinase inhibitors (CKIs). They specifically inhibit cell cycle kinase activity and the phosphorylation of Rb to arrest cells in the G_0/G_1 phase.[4,5] During EMT, the TGF-β signaling pathway is very important. Previous studies had found that high glucose caused renal parenchymal cell cycle arrest. And it also increased TGF-β expression, leading to EMT and interstitial fibrosis.[3] Whether the arrested cell cycle accelerates the process of EMT is the core subject of our research. If the recovery of cell cycle could improve EMT, it should offer a new way to treat renal fibrosis.

Nearly half of patients with diabetes are associated with hyperuricemia. Glomerular sclerosis and interstitial fibrosis are the main characteristics of these patients, who also often suffer from uric acid (UA) salt crystals. Thus, we used high concentrations of glucose and UA to induce a human renal proximal tubular epithelial cell damage model and a mouse model of diabetes with high UA to imitate the real state in DN patients.

The transplantation of mesenchymal stem cells (MSCs) could significantly improve renal damage and promote renal repair.[6] Some researches displayed that MSCs directly differentiate into renal tubular epithelial cells and promote renal repair.[7] However, most scholars believed that the paracrine mechanism was more important than the direct effect of MSCs in the process of repair.[8,9] MSC-conditioned medium was verified to contain microvesicles (MVs).[10] MVs are released from MSCs under conditions of rest, hypoxia stress, apoptosis, and shear stress and have a subcellular and heterogeneous structure. MVs are internalized into the target cells shuttling the surface receptors, proteins, bioactive lipids, mRNAs, and microRNAs to the cells, which regulate cell growth and differentiation. The miRNAs delivered by MV could regulate cell growth and differentiation. MicroRNA-451a (miR-451a) was first found in 2005 by Altuvia et al.[11] and located in chromosome 17qll.2. MiR-451a is related with the regulation of the hematopoietic system, differentiation, epithelial cell polarity formation, and other processes.[11] The target genes of miR-451a include calcium-binding protein, eukaryotic translation elongation factor, and the F-box protein family, which participates in the process of DN. It is the most highly expressed miRNAs in MV.[11]

The research aims to study how miR-451a in MSC–MVs restarts the blocked cell cycle of HK-2 and retards the progress of EMT and to explain the mechanism of renal injury repair.

Methods

Isolation of MVs from human MSCs and fibroblasts

Human umbilical MSCs were obtained from the Sichuan Stem Cell Bank & Sichuan Neo-Life Stem Cell Biotech Inc. MSCs were analyzed for immunophenotype by flow cytometry. MSCs expressed typical MSCs markers without hematopoietic markers and costimulatory molecules. The adipogenic differentiation and osteogenic differentiation of MSCs were determined as described previously.[12] Human foreskin fibroblasts (HFFs) were derived from the dermis[13] and used as a control. MSCs and HFFs were cultured in DMEM containing 10% FBS (Gibco), which was ultracentrifuged at 100,000*g* for 1 h at 4°C (Backman Coulter, Optima L-100K) to remove MVs in FBS before use. MVs were isolated from culture supernatants. To remove debris and dead cells, the supernatants were centrifuged at 500*g* at 4°C for 10 min, 2000*g* at 4°C for 15 min, and then 10,000*g* at 4°C for 30 min. The cell-free supernatants were ultracentrifuged twice at 100,000*g* at 4°C for 1 h. The protein concentration was analyzed by BCA methods (Beyotime Biotechnology).

Identification of MSC–MVs and analysis of the expression of miR-451a

The immunophenotype of MSC–MVs was analyzed by flow cytometry (Navios, Backman Coulter). Beads with sizes of 1.0 μm, 0.8 μm, and 0.4 μm, (Molecular Probes, Backman Coulter) were used as size markers. Flow cytometry was done as described previously (CD166, CD105, CD90, CD44, CD45, CD34, CD14, HLA-DR, Beckman Coulter).[8] Moreover, the Zetasizer Nano instrument (Malvern Instruments, Malvern Worcestershire, UK) and a dynamic light scattering particle size analyzer (LB-550, Horiba, Japan) were used to measure the size of MVs.

The 100,000*g* fraction of vesicles was suspended in 50–100 μL of 2% paraformaldehyde and deposited in plastic chamber slide wells. Vesicles were left to adhere to the plastic at room temperature overnight. If not completely dry, the excess liquid was removed, and the vesicles were post-fixed in 2.5% glutaraldehyde at 4°C for 10 min and dehydrated in ethanol. The cover of the chamber slide was removed, and the slide was coated with gold via sputtering for further observation by scanning electron microscopy.

RNAs were extracted from MSC–MVs and MSCs. The miR-451a level was tested using q-PCR using the SYBR Green PCR Kit (Ribo, China) and StepOneTM Real Time System (Bio-Rad, USA). Water was used as negative controls. The expression of miRNA between cells and MVs was compared based on the relative expression data. The results were normalized against one of the most stable miRNAs identified between cells and MVs.[14] Furthermore, we also used external references (39-3p) to compare miRNA levels between MVs and MSCs. The fold change in miRNA expression between the cells and the MVs was calculated based on the normalized mean differences ($2^{-\triangle\triangle Ct}$).

Experimental treatment of human renal proximal tubular epithelial cells

Human renal proximal tubular epithelial cells (HK-2, ATCC® Number: CRL-2190™) were cultured in DMEM containing 10% FBS (Gibco, Burlington, Canada) at 37°C in 95% air-5% CO_2. The injured HK-2 was established with high glucose (30 mM) and/or high UA (10 mg/dL). For the in vitro study, HK-2 cells (1×10^5) were treated in one well of six-well plate as the following groups: (1) 5.5 mM glucose control (NG); (2) 30 mM glucose + 10 mg/dL UA (GU); (3) GU + 30 μg MVs (MV); (4) GU+ 100 nM miR-451a mimic (RiboBio, China) (m); (5) GU + 100 nM miR-451a inhibitor (RiboBio, China) (I); and (6) GU+MV + 100 nM miR-451a inhibitor (VI). There were several control groups: 5.5 mM glucose + 25 mM D-mannitol (D, osmotic control); HFF-MVs (H); transfection reagent control; mimic and inhibitor control groups. All experiments were performed on cells from passages 3–8 with 80–90% confluence.

Cell viability and cell cycle analysis

CCK-8 Assay Kit was used to determine cell viability (Dojindo Molecular Technologies) according to the manufacturer's protocol.

Cell proliferations were tested with BrdU detection (Roche). The absorbance was tested by microplate reader (BioTek) at a wavelength of 370 nm.

After treatment, cells were collected and permeabilized overnight in 75% ethanol, then incubated with RNase (200 μg/ml) and PI (100 μg/ml) for 30 min at 4°C. The proliferation rate determined followed the equation proliferation rate=$(S+G_2/M)/(G_0/G_1+S+G_2/M)$.

Real-time PCR quantification

Total RNA of HK-2 cells was extracted by Tripure isolation reagent (Roche) and reverse transcribed to cDNA via first-stand cDNA synthesis kit using random primers (Roche). qPCR was performed to analyze P15, P19, E-cadherin, α-SMA using SYBR Premix Ex Taq (Takara Bio) (Table 1), and miR-451a using the SYBR Green PCR Kit (Ribo, China). The $2^{-\triangle\triangle Ct}$ method was performed for data analysis.

Western blotting

Proteins were extracted from HK-2 cells with a lysis buffer containing PMSF. Proteins run on SDS/PAGE and transferred to polyvinylidene difluoride membranes. The membranes were probed with antibodies against P15, P19, E-cadherin, and α-SMA (cat. NB100-91906, NB; ab102842, abcam; 610181, BD; ab5694, abcam) at 4°C overnight. After incubation with 1:2000 secondary antibody, the proteins were visualized by the Molecular Imager Gel Doc XR System (Bio-Rad).

Table 1. Primers for qPCR.

miR-451a	F: ACCGTTACCATTACT
	R: CTCACACGACTCACGA
p15INK4b	F: CCACTACCGTAAATGTCCAT
	R: AAGAAATGCCCACATGAATG
p19INK4d	F: AGTCCAGTCCATGACGCAG
	R: ATCAGGCACGTTGACATCAGC
E-cadherin	F: ATTTTTCCCTCGACACCCGAT
	R: TCCCAGGCGTAGACCAAGA
α-SMA	F: CACTGCCTTGGTGTGTGACAAT
	R: CGTAGCTGTCTTTTTGTCCCATTC

Luciferase reporter assay

Human p15 3′-UTR (1530 bp) and p19 3′-UTR (693 bp) with a mutation of the miR-451a seed sequence (p15:WT820–826 5′-AACGGUU-3′, mutant 820-826 5′-TTGCCAA-3′; p19: WT240–246 5′-AACGGUU-3′, mutant 240-246 5′-TTGCC AA-3′) were amplified by PCR (Tables 2 and 3) and cloned into the firefly and Renilla luciferase reporter vector pmiR-RB-REPORT (RiboBio Co., Ltd) predigested with Xho I and Not I. The 293T cells were seeded on 24-well plates with a density of 1×10^5 cells/well and transfected with luciferase reporter vectors (30 ng). Twenty-four hours after transfection, firefly and Renilla luciferase activities were measured, according to the manufacturer's manual (Promega). The renilla luciferase signal was normalized to the firefly luciferase signal for each individual analysis.

Mouse model of DN with hyperuricemia and treatments by MSC–MV-miR-451a

Studies were conducted following the National Institute of Health Guide for the Care and Use of Laboratory Animals. After two weeks of adaptive feeding, the 36 male Babl/c mice (8 to 10 weeks old) were divided into the following four groups, randomly following the principle of weight: (i) normal control group (N, n = 9), (ii) diabetes mellitus with high UA group (GU, n = 9), (iii) intervention with MSC–MVs in GU mice (MV, n = 9), and (iv) intervention with miR-451a agomir in GU mice (agomir, n = 9, RiboBio, China). Mice were induced diabetes by a single intraperitoneal injection with STZ (180 mg/kg). After 72 h, the tail blood was tested. Blood glucose above

Table 2. Primers for luciferase reporter assay.

p15-3′UTR	F: GCGGCTCGAGCAGGATGCTGGCCTTTGCT
	R: AATGCGGCCGCTAGGTGTGTTGGGGGGGGT
p15-mut	F: TAAATATATTGCCCAATGTTTGAAAACTATTTTA
	R: TTCAAACATTGGCAATATATTTACTAGAAGTTA
p19-3′UTR	F: GCGCTCGAGCTCAGGACCTCGTGGACATC
	R: AATGCGGCCGCGTGTAACTCTCCATCCCAGA
p19-mut	F: GCCACCTATTGCCAACAGTTTCTTCTGCGCCTC
	R: AGAAACTGTTGGCAATAGGTGGCTGTGGCCTGC

Table 3. Predicted consequential pairing of target region (top) and miRNA (bottom).

Position 820-827 of p15-3′UTR	5′...AGUGAGAGCAAUUGUAACGGUUA...
hsa-miR-451a	3′... UUGAGUCAUUACCAUUGCCAAA...
Position 240-246 of p19-3′UTR	5′...GGCCACAGCCACCUUAACGGUUC...
	3′... UUGAGUCAUUACCAUUGCCAAA...

16.7 mM was regarded as a diabetes model. Potassium oxonate (PO, 400 mg/kg) and adenine (25 mg/kg) were administered by intragastric administration once daily until they were sacrificed. The concentration of UA above 0.2 mg/dL was regarded as a hyperuricemia model. MVs (1.5 mg/kg) and agomir (0.5 mmol/kg) were injected at the tail vein to sacrifice the mice at each weekly time point.

Nine mice were killed in each group at each time point (five weeks, seven weeks, and nine weeks). Renal function was monitored (serum urea nitrogen, creatinine, glucose, and UA). To observe the pathological changes in kidney tissue, HE staining, Masson staining, and immunohistochemistry (P15, P19, E-cadherin, and α-SMA) were performed. q-PCR and WB were used to detect the expression level. The expression of markers was measured using Image-Pro-plus 6.0 software (Media Cybernetics, Inc.) to analyze the integral optical density. Fluorescence microscopy was used to ensure that fluorescence MVs could implant into the damaged renal tissue.

Statistical analysis

Results were expressed as the means ± SD from at least three independent experiments. SPSS version 19.0 (SPSS Inc.) was used for statistical analysis, and comparisons between two groups were measured using Student's t-test. A two-sided $P < 0.05$ was considered statistically significant.

Results

Characterization of MSC–MVs

Under scanning electron microscopy, MSC–MVs appeared as round or oval vesicles. The size of MVs ranged from tens to hundreds nanometers (Figure 1(a)), and their sizes were subjected in two sub-regions: near 30 nm (13.8%) and 300 nm (86.2%) (Figure 1(b)). The forward scatter signal tested MSC–MVs (Figure 1(c)). CD166, CD105, CD90, and CD44 were positive, which were known to be expressed on the MSC membrane as adhesion molecules; CD45, CD34, CD14, and CD80 were negative (Figure 1(d)). The expression level of miR-451a in MVs was 4.87 ± 2.03 fold higher than that in MSCs ($P = 0.032$).

MSC–MV-miR451a could decrease HK-2 damage induced by high glucose and UA

Cell viability was significantly decreased in the GU group (GU, 75.01% ± 0.61%), and the rate was further reduced by addition of the miR-451a inhibitor (I, 72.03% ± 0.66%). Cell activity significantly increased after MSC–MVs (MV) and miR451a mimic treatment (M) (97.30% ± 0.94%; 97.00% ± 0.69%; compared to the GU group, $P < 0.05$). However, in the VI group, the cell viability reduced to 79.30% ± 0.75%. No difference existed between the D-mannitol group (hypertonic control D, 97.73% ± 0.92%) and the control group ($P > 0.05$). The MVs secreted by fibroblasts (H) did not differ from the GU group in terms of cell viability ($P > 0.05$) (Figure 2(a)). Cell proliferative rate showed the same changing trend (Figure 2(b)).

Compared with the normal control group (proliferation index 47.85% ± 0.15%), the proliferation index of the GU group was reduced to 38.20% ± 0.52% ($P = 0.001$) and then decreased to 37.29% ± 0.42% by the addition of inhibitor (I). However, the addition of MSC–MVs and mimics both could increase the proliferation index to 46.50% ± 0.11% and 46.22% ± 0.02% (compared to GU, $P < 0.05$), respectively. The VI group showed a lower index (39.08%

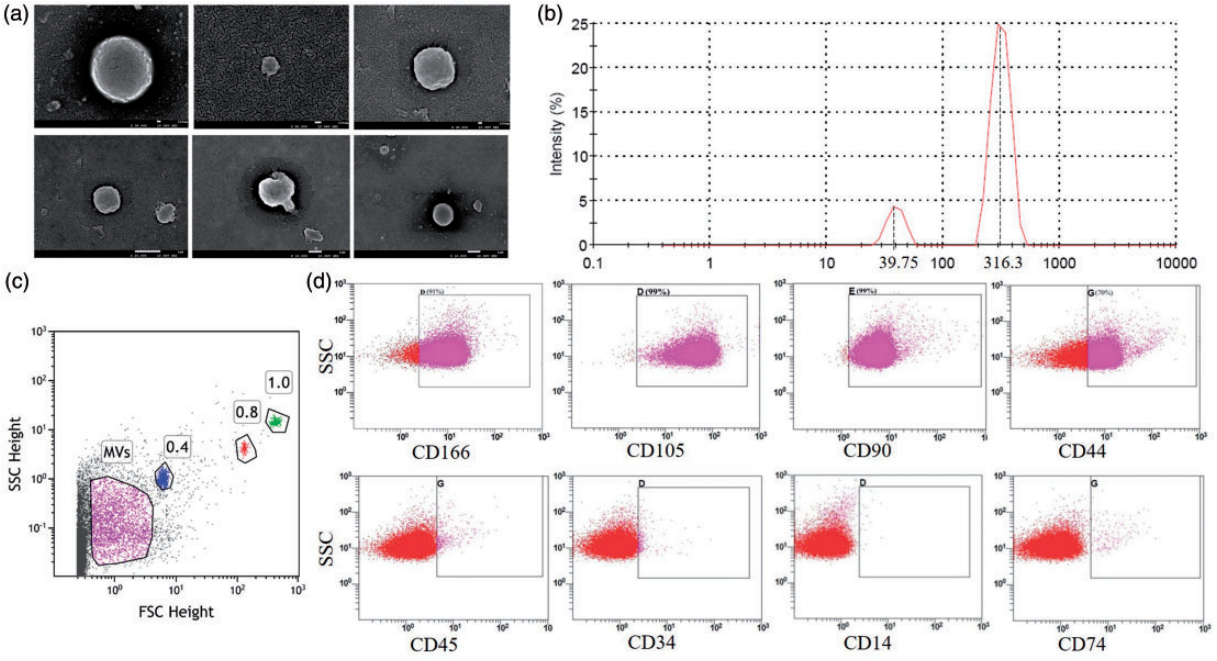

Figure 1. Characteristics of MSC–MVs. (a) Image of MSC–MVs scanning by electron microscopy (scale: upper 100 nm, lower 1 μm). (b) Cumulative distribution graph of MSC–MVs. (c) Microspheres distinguished the MV particle size (using 1.0 μm, 0.8 μm, and 0.4 μm standard microspheres). (d) Immunophenotypic identification of MSC–MVs (upper: MSC–MVs, lower: isotype). (A color version of this figure is available in the online journal.)

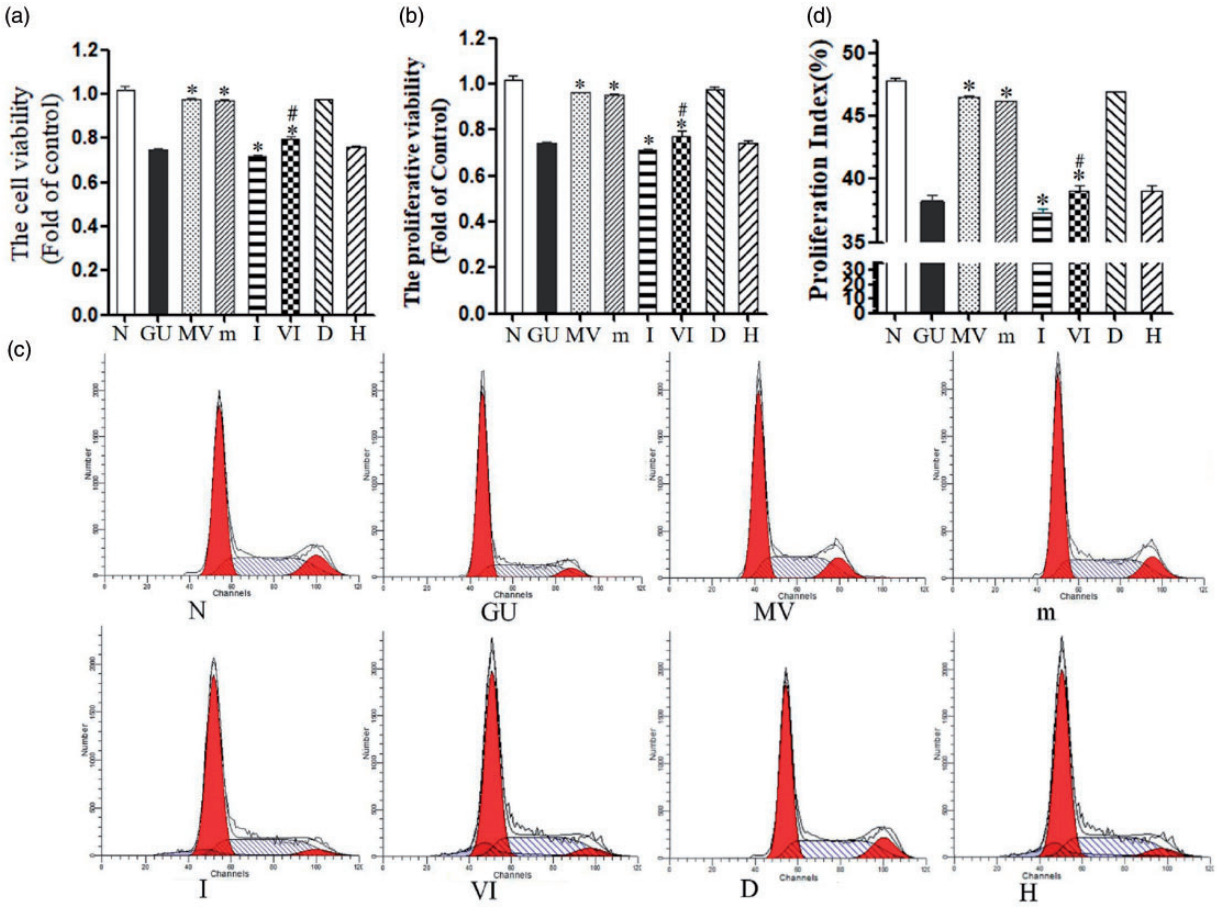

Figure 2. Ameliorated effect of MV-miR-451a on HK-2. (a) Cell viability was determined using the CCK-8 assay, and data are expressed as a percentage of the control. (b) HK-2 proliferative ability via BrdU. (c) Cycle changes using control reagent. (d) Representative FACS cell cycle histograms. $^{*}P < 0.05$, compared with GU group; $^{\#}P < 0.05$, compared with MV group. N: 5.5 mM glucose control, GU: 30 mM glucose + 10 mg/dL uric acid, MV: GU + 30 μg MVs, m: GU+100 nM miR-451a mimic, I: GU + 100 nM miR-451a inhibitor, VI: GU+MV + 100 nM miR-451a inhibitor, D: 5.5 mM glucose + 25 mM D-mannitol, H: MVs from Human foreskin fibroblasts (HFF). (A color version of this figure is available in the online journal.)

$\pm 0.38\%$) than MV. At the same time, the cell cycle of the D-mannitol group showed no obvious change compared to the normal control group ($P > 0.05$). There was no significant difference between MVs secreted by fibroblasts (H) and the GU group ($P > 0.05$) (Figure 2(c) and (d)).

At 24 h, miR-451a in the GU group fell to 0.26 ± 0.11-fold of normal control ($P = 0.005$). miR-451a in MSC–MVs group was 6.54 ± 0.08-fold higher than the control group. In the high glucose and UA group (GU), P15 increased to 2.81 ± 0.14-fold; P19 increased 4.71 ± 0.15-fold; E-cadherin decreased to 0.31 ± 0.05-fold; and α-SMA increased 6.36 ± 0.68-fold (compared to N, $P = 0.001$, 0.001, 0.0002, 0.007). After addition of the inhibitor (I), the expression of p15 (2.12 ± 0.16), p19 (1.13 ± 0.04) and α-SMA (3.26 ± 0.40) decreased in the presence of mimic (m), but the expression of E-cadherin increased (0.59 ± 0.06) (compared with GU, $P < 0.05$). However, the effect of improvement from MSC–MV was counteracted by inhibitor (VI) (Figure 3(a)). These markers' protein expression levels were consistent with mRNA levels (Figure 3(b) and (c)).

The 3′-UTR luciferase reporter assays were used to assess the direct repression of miR-451a. Luciferase activity in cells (containing WT vector) was reduced in response to miR-451a in both P15 and P19. In a separate experiment, miR-451a was transfected into a mutant vector and showed no change in luciferase activity. Furthermore, a miR-451a mimic control did not change the values in WT vector and Mut vector. These results indicate that miR-451a directly repressed p15 and p19 via 3′-UTR (Figure 3(d)).

MSC–MV-miR451a reduced renal fibrosis in diabetic mice with high UA model in vivo

The blood glucose in the GU group was 44.88 ± 3.16 mmol/L (normal control group 6.19 ± 1.03 mmol/L, $P < 0.01$). The UA level in the GU group was 1.88 ± 0.38 mg/dL (normal control 0.21 ± 0.07 mg/dL, $P < 0.01$) (Figure 4(a)). During the experiment, urea nitrogen (urea) and serum creatinine (crea) increased gradually in the GU group, but administration of MV or miR-451a (agomir) decreased the urea and crea levels. After eight weeks, urea increased to 62.33 ± 1.82 mmol/L but declined to 35.65 ± 1.06 mmol/L in MV and 36.33 ± 0.85 mmol/L in agomir (compared to GU, $P < 0.05$). Crea increased to 117.28 ± 1.67 μmol/L in GU, but decreased to 57.37 ± 1.97 μmol/L in MV and 72.98 ± 1.94 μmol/L in agomir (compared to GU, $P < 0.05$) (Figure 4(b)).

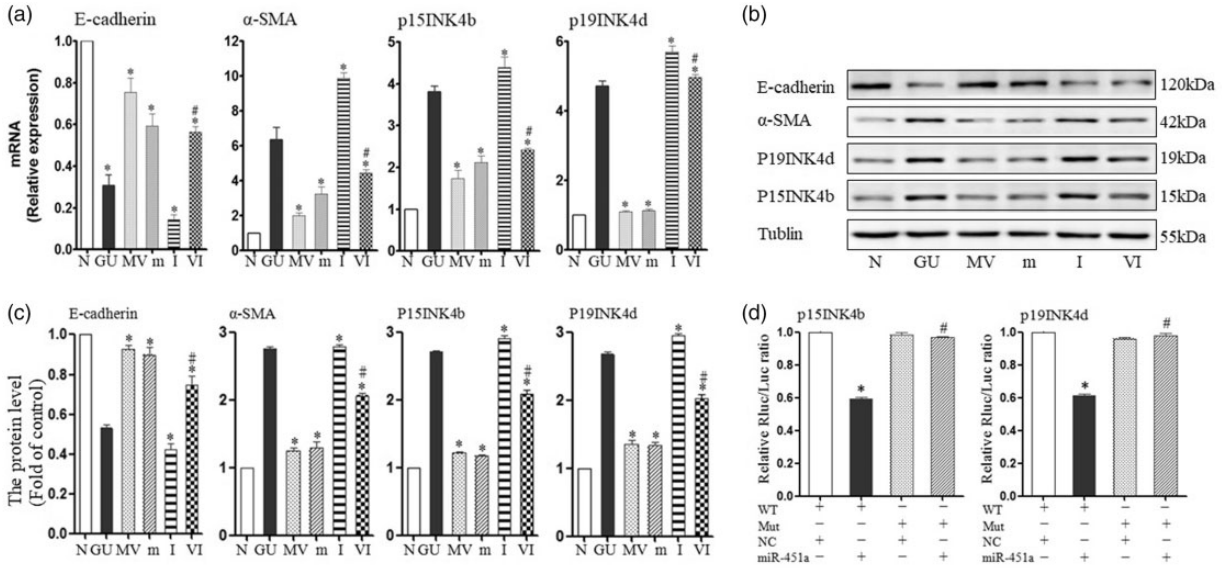

Figure 3. MSC–MVs regulated the process of EMT by inhibition of P15INK4b and P19INK4d through miR-451. (a) mRNA levels of markers from CKIs and EMT as measured by q-PCR. (b) Representative Western blotting of markers in miR-451a given either as MVs or a miR-451a mimic. (c) Protein levels of markers were quantified using ImageJ software. (d) Double luciferase reaction to verify the target gene: WT: wild type, Mut: mutant type, NC: normal control. N: 5.5 mM glucose control, GU: 30 mM glucose + 10 mg/dL uric acid, MV: GU + 30 μg MVs, m: GU+100 nM miR-451a mimic, I: GU + 100 nM miR-451a inhibitor, VI: GU+MV + 100 nM miR-451a inhibitor.

The expression levels of α-SMA were 7.14 ± 0.13-fold (GU), 2.12 ± 0.25-fold (MV), and 2.44 ± 0.06-fold (agomir), respectively (compared with GU, $P < 0.05$). Nevertheless, E-cadherin in the GU group was only 0.42 ± 0.03-fold of the control. MV and agomir improved E-cadherin level to 0.83 ± 0.03-fold and 0.80 ± 0.02-fold (compared to GU, $P < 0.05$) (Figure 4(c)), respectively. Conversely, α-SMA decreased after treatment with MV and agomir, and the expression of E-cadherin improved (compared to the GU group, $P < 0.01$) (Figure 4(d) and (e)).

The DM mice with high UA injury showed serious pathological changes in following eight weeks: from the mild volume increase to visible scar-like changes in the general specimen, from vacuole and particle denaturation to flattened even flaky or diffuse atrophy in renal tubular epithelial cells, gradual expansion in the lumen, and protein cast gradually increased, from mononuclear cell infiltration to focal and even multifocal fibrosis in renal interstitial tissue (Figure 4(f)). The pathological changes in the process, i.e. immunohistochemistry showed similar trends: α-SMA increased gradually, while E-cadherin showed a decreasing trend. And MVs and agomir could reverse this trend (Figure 4(g)). MV and agomir interventions significantly improved renal pathology in DM mice.

MSC–MV-miR451a reduced renal fibrosis through down-regulation of the P15INK4b and P19INK4d

The expression of miR-451a in the GU model significantly decreased to $6.73\% \pm 0.82\%$ of the N group ($P < 0.01$). However, after infusion of MV for eight weeks, the level of miR-451a increased to $61.01\% \pm 3.51\%$ (compared to GU, $P < 0.01$) (Figure 5(a)).

The expression of P15 in kidneys of DM mice was 6.10 ± 0.16-fold of the normal control. DM mice treated with MV or agomir were only 1.31 ± 0.08-fold and 1.57 ± 0.06-fold (compared with GU, $P < 0.05$). The expression levels of p19 were 3.52 ± 0.05-fold (GU), 1.47 ± 0.05-fold (MV), 1.65 ± 0.03-fold (agomir), respectively (compared to GU, $P < 0.05$) (Figure 5(b)). After eight weeks, the protein expression of P15 and P19 was markedly up-regulated, while the expression of E-cadherin was down-regulated in the kidney of the GU group. By contrast, the expression of P15 and P19 decreased after treatment with MV and agomir. MV showed better protective effect than that of agomir (compared to the GU group, $P < 0.01$) (Figure 5(c) and (d)).

The expression of P15 and P19 in kidney increased gradually. But MVs and agomir could reverse this trend (Figure 5(e) and (f)).

Discussion

In the present study, we demonstrated that miR-451a was enriched in MSC–MVs. MSC–MVs-miR-451a could specifically inhibit P15 and P19 to restart the blocked cell cycle. Furthermore, it could improve EMT by regulating E-cadherin and α-SMA. It verified that cell cycle was associated with EMT.

At present, clinical and epidemiological data indicate that 35% to 50% of patients with diabetes were complicated with hyperuricemia.[15] There were so many mechanisms of hyperuric acid aggravating DN.[16–18] NO was one of them. Hyperuricemia could reduce NO level by direct clearance of NO and inhibition of the dense spot NO synthase system. Insulin was partly dependent on NO mediation to take up glucose, and high blood UA levels increased insulin resistance. In addition, UA deposition in the organization would cause direct toxic effects, such as inflammation and increased expression of TNF-α[19] and TGF-β.[20]

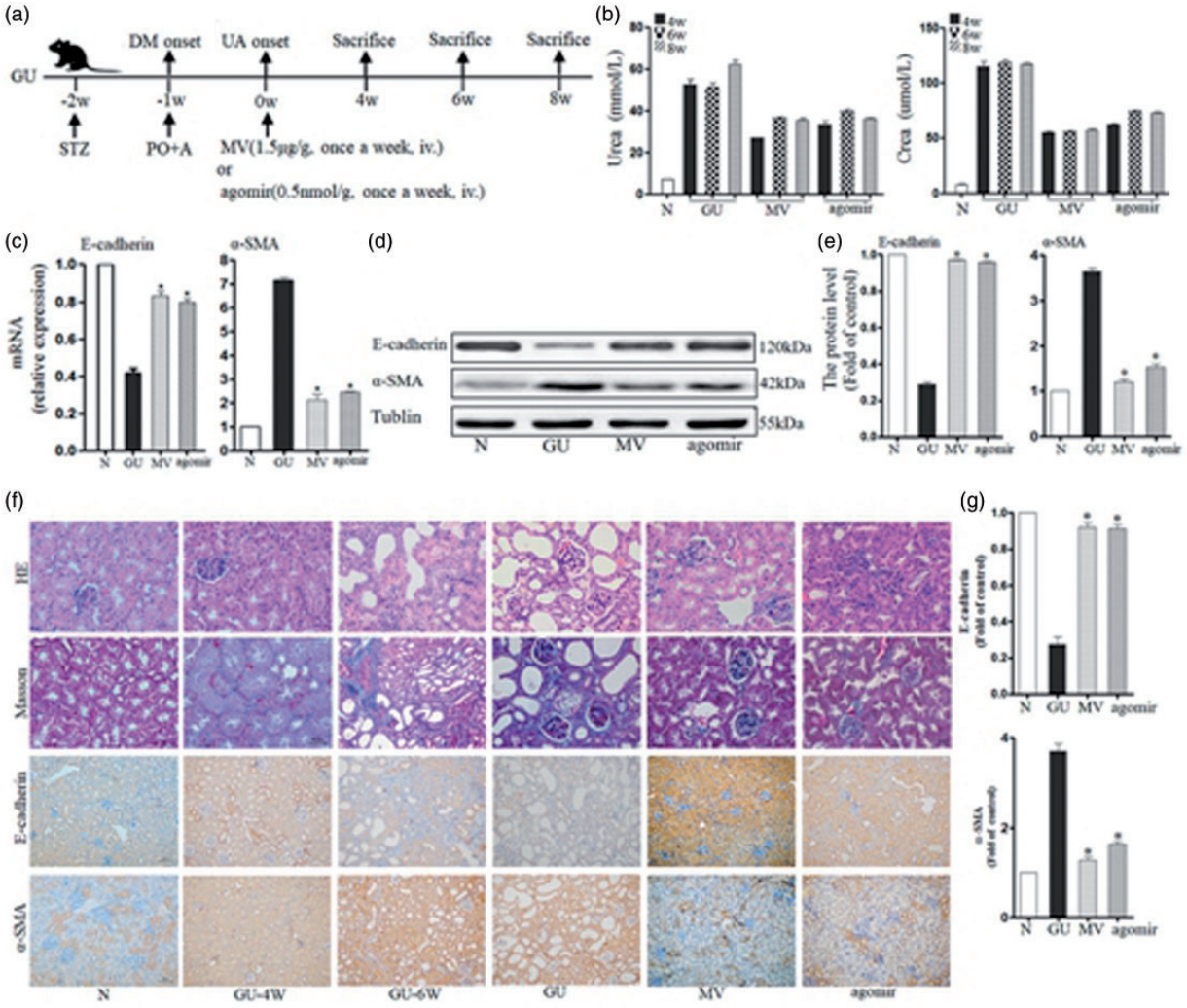

Figure 4. Effects of MSC–MVs-miR-451a on EMT in mice with diabetes and hyperuricemia: (a) The experimental design in vivo: STZ-induced diabetic rats and with hyperuricemia were treated with MVs (1.5 mg/kg) or agomir (0.5 mmol/kg) once a week. (b) Dynamic variation in renal function (urea and crea) in Babl/c mice with high glucose and uric acid during the process of damage or repairmen. (c) mRNA levels of EMT-related markers, including E-cadherin and α-SMA, were determined by q-PCR in kidneys. Data are expressed as a percentage of the control. (d) Representative Western blotting of EMT markers (E-cadherin and α-SMA) in GU, MV, and agomir group. (e) Protein levels of EMT markers were quantified using ImageJ software. (f) Representative micrographs of histology for kidney sections with HE (×40), Masson (×40) and immunohistochemistry of E-cadherin and α-SMA (×20). (g) Protein levels of EMT markers from renal immunohistochemistry were quantified using Image-pro Plus software. *$P < 0.05$ vs. GU group. N: normal control group, GU: diabetes mellitus with high uric acid group, MV: intervention with MSC–MVs in GU mice, agomir: intervention with miR-451a agomir in GU mice. (A color version of this figure is available in the online journal.)

In type 2 diabetes mellitus, lowering blood UA could alleviate microalbuminuria and tubulointerstitium.[21,22] Therefore, we set up compound model of high glucose and high UA in order to mimic the real progression of DN patients.

Renal cell damage in DN renal fibrosis was often associated with cell cycle stagnation.[23] High glucose can induce renal tubular epithelial cells to produce excess ROS,[24–29] which damages DNA and inevitably stages cell cycle.[30,31] P15 and P19 belong to CKIs, which specifically inhibit the activity of CDK4 via its characteristic ankyrin repeat sequence.[32,33] P15 and P19 are often considered as tumor suppressors.[34] However, they also have multiple biological functions, such as regulating stem cell differentiation, apoptosis, and DNA damage.[5] DNA damage activates P15 and P19 at the transcriptional level to inhibit the CDK4-6/cyclinD/pRb signaling pathway, stage the cell cycle in the G_0/G_1 phase, and stop replication to enter an irreversible growth stagnation state.[35] In this study, P15 and P19 were induced to up-regulated by high glucose both from mRNA levels and protein levels. And they down-regulated the cell viability, proliferative rate, and staged cell cycle before check-point, which is consistent with other studies.

The relationship of cell cycle arrest and EMT in renal interstitial fibrosis is still unclear. TGF-β-induced EMT acts mainly through the β-integrin signaling pathway to promote Smad molecular transcription. TGF-β forms a complex with Smad2, 3, and 4, which binds to transcription factors (Snail family, ZEB family, and bHLH family) to regulate the transcription of target genes, inhibit epithelial cell markers (E-cadherin), and activate stromal cell markers (α-SMA).[36,37] It has been found that high glucose can cause cell cycle arrest in renal parenchymal cells, in which TGF-β expression increased and developed into

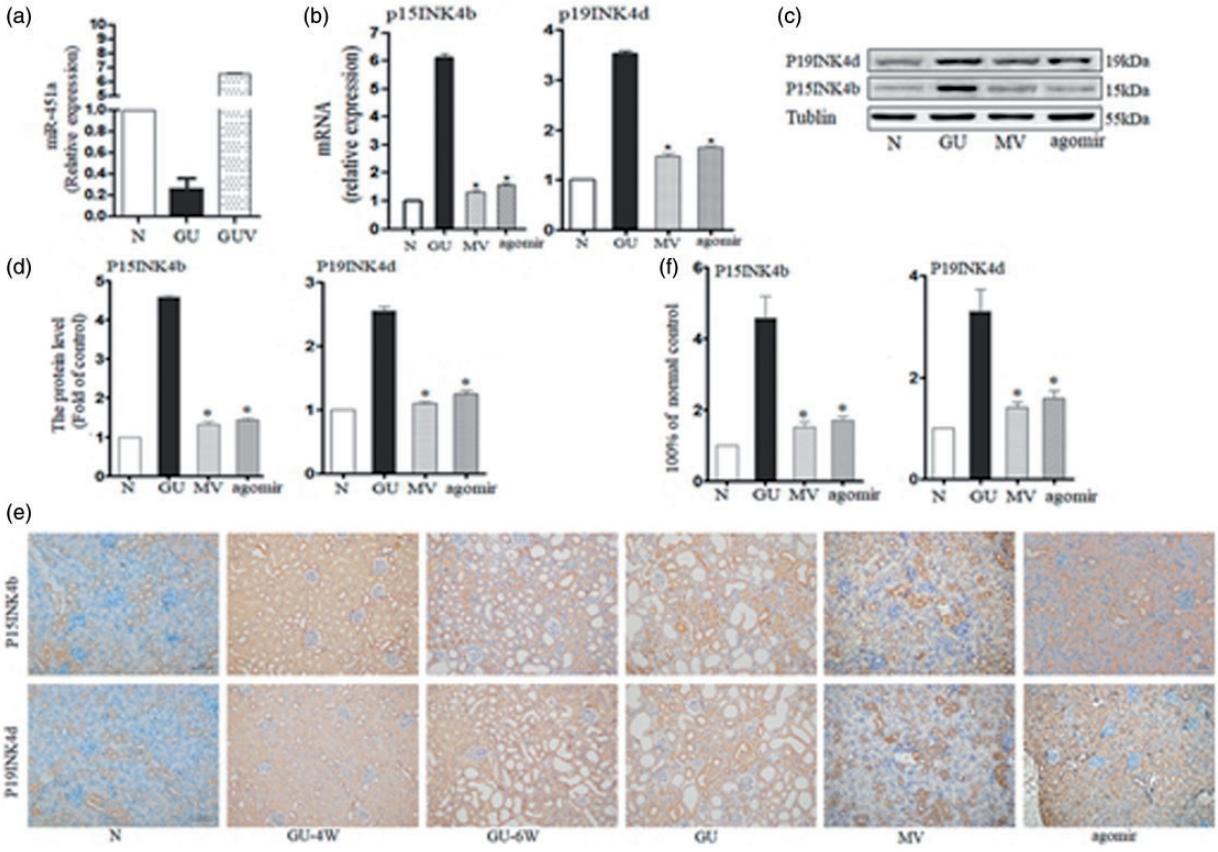

Figure 5. MSC–MVs-miR-451a inhibited EMT by inhibiting CKIs through the p15 INK4b and p19INK4d in mice with diabetes and hyperuricemia: (a) The changes of miR-451a expression level in different groups (b) mRNA levels of EMT-related markers, including p15INK4b and p19INK4d, were determined by q-PCR in treated kidneys. (c) Representative Western blotting of markers given either MVs or agomir. (d) Protein levels of markers were quantified using ImageJ software. (e) Representative micrographs of immunohistochemistry of P15INK4b and P19INK4d (×20). (f) Protein levels of markers were quantified using Image-pro Plus software. *$P < 0.05$ vs GU group. N: normal control group, GU: diabetes mellitus with high uric acid group, MV: intervention with MSC–MVs in GU mice, agomir: intervention with miR-451a agomir in GU mice. (A color version of this figure is available in the online journal.)

EMT and interstitial fibrosis.[38] The TGF-β/Smad3-4 signaling pathway promotes the expression of p15.[39] Whether the delayed cell cycle is an accelerated EMT process is the subject of our research and a key step in emerging treatment. In this study, hyper glucose and hyperuricemia stopped cell cycle, and also produced EMT. MSC–MVs-miR-451a restarted the stagnant cell cycle, and then improved EMT. It implies that if the cell cycle is restored, EMT can be improved or even repaired, which would provide a new treatment for DN renal fibrosis.

Several studies demonstrated that MSC could alleviate renal damage including fibrosis in DN.[40,41] In renal tubules after injury, the number of MSC was low, which implies MSC exerts trophic effect on injured tubular cells, but not a direct repopulation.[42,43] Paracrine action may be the MSC's way to exert effects.[8,44–46] MV originates from the MSCs-derived medium, which is the subcellular structure released under certain conditions, and with heterogeneity.[47] At present, MSC–MVs have been served as a biological factors carrier, including protein (membrane receptor, ribosomal protein) and genetic material (mRNA, miRNA).[48] MSC–MV surfaces express not only common membrane proteins such as CD9 and CD81 but also express MSC-specific adhesion molecules, such as CD44 and CD29.[48] This coincides with our results, that MVs derived from MSCs have the same surface marker as MSC. These adhesion molecules are vital in entering target cells. Bruno et al.[14] showed that with anti-CD44 and CD29 antibody treatment, MSC–MVs no longer enter renal tubular epithelial cells. Furthermore, MSC–MVs contain specific nucleic acids, which have been reported to play a protective role in acute renal injury of non-SCID mouse models. MVs highly enriched miRNAs and shuttled them to target cells to exert protective effect.[50] The highly expressed miRNAs of MSCs included miR-223, miR-564, and miR-451a. In our study, miR-451a was verified to be enriched in MVs compared with MSCs. And the enriched miR-451a targeted p15 and p19 to restart cell cycle and slows down the process of EMT. On the other hand, researchers have found that miR-451a was down-regulated by the screening of microRNAs in the early phase of type 2 DN mice,[51] which was consisted with our results in DM mice. Ywhaz had been reported as one of the target genes of miR-451a, which mediates the insulin receptor and p38MAPK signaling pathway to protect the glomerular hypertrophy.[51] We found CKIs were the new targets of miR-451a. miR-451a inhibited p15 and p19 by binding to their 3′-UTR. And it made some effect on cell cycle and EMT.

Taken together, our data demonstrate that miR-451a shuttled by MSC–MVs is one of their effectors to repair

fibrosis in DN with hyperuricemia. And we propose that miR-451a regulates cell cycle by targeting p15 and p19 and ameliorates EMT. The research provides a rationale for incorporating miR-451a into current prognostic and therapeutic marker in DN.

Authors' contributions: LZ, WGZ, YRL participated in the design; All the authors did interpretation of the studies, analysis of the data, review of the manuscript, and conducted the experiments; LZ, WGZ, YRL wrote and revised the article.

DECLARATION OF CONFLICTING INTERESTS

The author(s) declared the following potential conflicts of interest with respect to the research, authorship, and/or publication of this article: LZ has been employed by Sichuan Academy of Medical Sciences and Sichuan Provincial People's Hospital, and achieved the degree of PhD in Sichuan University. Others have nothing to declare.

FUNDING

The author(s) disclosed receipt of the following financial support for the research, authorship, and/or publication of this article: This study was supported by the National Natural Science Foundation of China (grant numbers: 81370824 and 31571474) and Hospital foundation of Sichuan Academy of Medical Sciences and Sichuan Provincial People's Hospital (30305030864).

ORCID iD

Yanrong Lu http://orcid.org/0000-0002-3728-222X

REFERENCES

1. Yang W, Lu J, Weng J, Jia W, Ji L, Xiao J, Shan Z, Liu J, Tian H, Ji Q, Zhu D, Ge J, Lin L, Chen L, Guo X, Zhao Z, Li Q, Zhou Z, Shan G, He J. China National Diabetes and Metabolic Disorders Study Group. Prevalence of Diabetes among Men and Women in China. *N Engl J Med* 2010;**362**:1090–101
2. Bianchi F, Sala E, Donadei C, Capelli I, La Manna G. Potential advantages of acute kidney injury management by mesenchymal stem cells. *World J Stem Cells* 2014;**6**:644–50
3. Tasanarong A, Kongkham S, Khositseth S. Dual inhibiting senescence and epithelial-to-mesenchymal transition by erythropoietin preserve tubular epithelial cell regeneration and ameliorate renal fibrosis in exposed to high glucose. *Biomed Res Int* 2013;**2013**:308130
4. Cánepa ET, Scassa ME, Ceruti JM, Marazita MC, Carcagno AL, Sirkin PF, Ogara MF. INK4 proteins, a family of mammalian CDK inhibitors with novel biological functions. *IUBMB Life* 2007;**59**:419–26
5. Carcagno AL, Giono LE, Marazita MC, Castillo DS, Pregi N, Cánepa ET. E2F1 induces p15INK4b, a protein involved in the DNA damage response, following UV irradiation. *Mol Cell Biochem* 2012;**366**:123–9
6. Li Calzi S, Neu MB, Shaw LC, Grant MB. Endothelial progenitor dysfunction in the pathogenesis of diabetic retinopathy: treatment concept to correct diabetes- associated deficits. *EPMA J* 2010;**1**:88–100
7. Tan X, Gong YZ, Wu P, Liao DF, Zheng XL. Mesenchymal stem cell-derived microparticles: a promising therapeutic strategy. *Int J Mol Sci* 2014;**15**:14348–63
8. Bruno S, Grange C, Deregibus MC, Calogero RA, Saviozzi S, Collino F, Morando L, Busca A, Falda M, Bussolati B, Tetta C, Camussi G. Mesenchymal stem cell-derived microvesicles protect against acute tubular injury. *J Am Soc Nephrol* 2009;**20**:1053–67
9. Strassburg S, Hodson NW, Hill PI, Richardson SM, Hoyland JA. Bi-directional exchange of membrane components occurs during co-culture of mesenchymal stem cells and nucleus pulposus cells. *PLoS One* 2012;**7**:e33739
10. Sokolovaa V, Ludwigb AK, Hornung S, Rotan O, Horn PA, Epple M, Giebel B. Characterisation of exosomes derived from human cells by nanoparticle tracking analysis and scanning electron microscopy. *Colloids Surf B Biointerfaces* 2011;**87**:146–50
11. Altuvia Y, Landgraf P, Lithwick G, Elefant N, Pfeffer S, Aravin A, Brownstein MJ, Tuschl T, Margalit H. Clustering and conservation patterns of human microRNAs. *Nucleic Acids Res* 2005;**33**:2697–706
12. Pittenger MF, Mackay AM, Beck SC, Jaiswal RK, Douglas R, Mosca JD, Moorman MA, Simonetti DW, Craig S, Marshak DR. Multilineage potential of adult human mesenchymal stem cells. *Science* 1999;**284**:143–7
13. Granot D, Kunz-Schughart LA, Neeman M. Labeling fibroblasts with biotin-BSA-GdDTPA-FAM for tracking of tumor-associated stroma by fluorescence and MR imaging. *Magn Reson Med* 2005;**54**:789–97
14. Collino F, Deregibus MC, Bruno S, Sterpone L, Aghemo G, Viltono L, Tetta C, Camussi G. Microvesicles derived from adult human bone marrow and tissue specific mesenchymal stem cells shuttle selected pattern of miRNAs. *PLoS One* 2010;**5**:e11803–18
15. Dobesh PP. Managing hyperurice in patients with type 2 diabetes mellitus. *Am J Health Syst Pharm* 2006;**63**:1140–9
16. Madero M, Sarnak MJ, Wang X, Greene T, Beck GJ, Kusek JW, Collins AJ, Levey AS, Menon V. Uric acid and long-term outcomes in CKD. *Am J Kidney Dis* 2009;**53**:796–803
17. Kodama S, Saito K, Yachi Y, Asumi M, Sugawara A, Totsuka K, Saito A, Sone H. Association between serum uric acid and development of type 2 diabetes. *Diabetes Care* 2009;**32**:1737–42
18. Li C, Han L, Levin AM, Song H, Yan S, Wang Y, Wang Y, Meng D, Lv S, Ji Y, Xu X, Liu X, Wang Y, Zhou L, Miao Z, Mi QS. Multiple single nucleotide polymorphisms in the human urate transporter1(hURAT1) gene are associated with hyperuricemia in Han Chinese. *J Med Genet* 2010;**47**:204–10
19. Zhu A, Zou T, Xiong G, Zhang J. Association of uric acid with traditional inflammatory factors in stroke. *Int J Neurosci* 2016;**126**:335–41
20. Yen JH, Lin LC, Chen MC, Sarang Z, Leong PY, Chang IC, Hsu JD, Chen JH, Hsieh YF, Pallai A, Köröskényi K, Szondy Z, Tsay GJ. The metastatic tumor antigen 1-trans-glutaminase-2 pathway is involved in self-limitation of monosodium urate crystal-induced inflammation by upregulating TGF-β1. *Arthritis Res Ther* 2015;**17**:65
21. Habu Y, Yano I, Okuda M, Fukatsu A, Inui K. Restored expression and activity of organic ion transporters rOAT1, rOAT3 and rOCT2 after hyperuricemia in the rat kidney. *Biochem Pharmacol* 2005;**69**:993–9
22. Jin M, Yang F, Yang I, Yin Y, Luo JJ, Wang H, Yang XF. Uric acid, hyperuricemia and vascular diseases. *Front Biosci (Landmark Ed)* 2012;**17**:656–69
23. Chkhotua AB, Abendroth D, Froeba G, Schelzig H. Up-regulation of cell cycle regulatory genes after renal ischemia/reperfusion: differential expression of p15(INK4b), p19(INK4d) and p27(Kip1) cyclin-dependent kinase inhibitor genes depending on reperfusion time. *Transplant Int* 2006;**19**:72–7
24. Sekar D, Venugopal B, Sekar P, Ramalingam K. Role of microRNA 21 in diabetes and associated/related diseases. *Gene* 2016;**582**:14–8
25. Slyvka Y, Malgor R, Inman SR, Ding J, Heh V, Nowak FV. Antioxidant diet and sex interact to regulate NOS isoform expression and glomerular mesangium proliferation in Zucker diabetic rat kidney. *Acta Histochem* 2016;**118**:183–93
26. Forbes JM, Coughlan MT, Cooper ME. Oxidative stress as a major culprit in kidney disease in diabetes. *Diabetes* 2008;**57**:1446–54
27. Yamagishi S-I, Matsui T. Advanced glycation end products, oxidative stress and diabetic nephropathy. *Oxidative Med Cell Longevity* 2010;**3**:101–8
28. Montero RM, Covic A, Gnudi L, Goldsmith D. Diabetic nephropathy: what does the future hold? *Int Urol Nephrol* 2016;**48**:99–113
29. Singh DK, Winocour P, Farrington K. Oxidative stress in early diabetic nephropathy: fueling the fire. *Nat Rev Endocrinol* 2011;**7**:176–84
30. Hakim FA, Pflueger A. Role of oxidative stress in diabetic kidney disease. *Med Sci Monit* 2010;**16**:RA37–48

31. Li Z, Pearlman AH, Hsieh P. DNA mismatch repair and the DNA damage response. *DNA Repair (Amst)* 2016;**38**:94–101
32. Kowluru RA, Kowluru A, Mishra M, Kumar B. Oxidative stress and epigenetic modifications in the pathogenesis of diabetic retinopathy. *Prog Retin Eye Res* 2015;**48**:40–61
33. Rani V, Deep G, Singh RK, Palle K, Yadav UC. Oxidative stress and metabolic disorders: pathogenesis and therapeutic strategies. *Life Sci* 2016;**148**:183–93
34. Cánepa ET, Scassa ME, Ceruti JM, Marazita MC, Carcagno AL, Sirkin PF, Ogara MF. INK4 proteins, a family of mammalian CDK inhibitors with novel biological functions. *IUBMB Life* 2007;**59**:419–26
35. Carcagno AL, Marazita MC, Ogara MF, Ceruti JM, Sonzogni SV, Scassa ME, Giono LE, Cánepa ET. E2F1-mediated upregulation of p19INK4d determines its periodic expression during cell cycle and regulates cellular proliferation. *PLoS One* 2011;**6**:e21938
36. Meng X, Ezzati P, Wilkins JA. Requirement of podocalyxin in TGFbeta induced epithelial mesenchymal transition. *PLoS One* 2011;**6**:e18715
37. Araki K, Shimura T, Suzuki H, Tsutsumi S, Wada W, Yajima T, Kobayahi T, Kubo N, Kuwano HE. N-cadherin switch mediates cancer progression via TGF-β-induced epithelial-to-mesenchymal transition in extrahepatic cholangiocarcinoma. *Br J Cancer* 2011;**105**:1885–93
38. Ksiazek K, Korybalska K, Jörres A, Witowski J. Accelerated senescence of human peritoneal mesothelial cells exposed to high glucose: the role of TGF-beta1. *Lab Invest* 2007;**87**:345–56
39. Thillainadesan G, Chitilian JM, Isovic M, Ablack JN, Mymryk JS, Tini M, Torchia J. TGF-β-dependent active demethylation and expression of the p15INK4b tumor suppressor are impaired by the ZNF217/CoREST complex. *Mol Cell* 2012;**46**:636–49
40. Lee RH, Seo MJ, Reger RL, Spees JL, Pulin AA, Olson SD, Prockop DJ. Multipotent stromal cells from human marrow home to and promote repair of pancreatic islets and renal glomeruli in diabetic NOD/SCID mice. *Proc Natl Acad Sci USA* 2006;**103**:17438–43
41. Ezquer F, Ezquer M, Simon V, Pardo F, Yañez A, Carpio D, Conget P. Endovenous administration of bone-marrow-derived multipotent mesenchymal stromal cells prevents renal failure in diabetic mice. *Biol Blood Marrow Transplant* 2009;**15**:1354–65
42. Humphreys BD, Bonventre JV. Mesenchymal stem cells in acute kidney injury. *Annu Rev Med* 2008;**59**:311–25
43. Romagnani P. Kidney regeneration: any prospects? *Contrib Nephrol* 2011;**170**:228–36
44. Tan X, Gong YZ, Wu P, Liao DF, Zheng XL. Mesenchymal stem cell-derived microparticles: a promising therapeutic strategy. *Int J Mol Sci* 2014;**15**:14348–63
45. Lai RC, Chen TS, Lim SK. Mesenchymal stem cell exosome: a novel stem cell-based therapy for cardiovascular disease. *Regen Med* 2011;**6**:481–92
46. Bruno S, Grange C, Collino F, Deregibus MC, Cantaluppi V, Biancone L, Tetta C, Camussi G. Microvesicles derived from mesenchymal stem cells enhance survival in a lethal model of acute kidney injury. *Plos One* 2012;**7**:e33115–26
47. Gatti S, Bruno S, Deregibus MC, Sordi A, Cantaluppi V, Tetta C, Camussi G. Microvesicles derived from human adult mesenchymal stem cells protect against ischaemia-reperfusion-induced acute and chronic kidney injury. *Nephrol Dial Transplant* 2011;**26**:1474–83
48. Mathivanan S, Fahner CJ, Reid GE, Simpson RJ. ExoCarta 2012: database of exosomal proteins, RNA and lipids. *Nucleic Acids Res* 2012;**40**:D1241–4
49. Tang Y, Wan W, Wang L, Ji S, Zhang J. microRNA-451 inhibited cell proliferation, migration and invasion through regulation of MIF in renal cell carcinoma. *Int J Clin Exp Pathol* 2015;**8**:15611–21
50. Zhang Z, Luo X, Ding S, Chen J, Chen T, Chen X, Zha H, Yao L, He X, Peng H. MicroRNA-451 regulates p38 MAPK signaling by targeting of Ywhaz and suppresses the mesangial hypertrophy in early diabetic nephropathy. *FEBS Lett* 2012;**586**:20–6
51. Bhatt K, Kato M, Natarajan R. Mini-review: emerging roles of microRNAs in the pathophysiology of renal diseases. *Am J Physiol Renal Physiol* 2016;**310**:F109–18

(Received August 9, 2018, Accepted November 25, 2018)